Archives of Materials Science and Engineering

Volume 48
Issue 2
April 2011
Pages 89-96

International Scientific Journal published monthly by the World Academy of Materials and Manufacturing Engineering

Characterization of the structure features of $CeZrO_2$ and $Ni/CeZrO_2$ catalysts for tar gasification with steam

A. Łamacz [a], M. Pawlyta [b,*], L.A. Dobrzański [b], A. Krztoń [a]

[a] Centre of Polymer and Carbon Materials, Polish Academy of Sciences, ul. M. Curie-Skłodowskiej 34, 41-819 Zabrze, Poland

[b] Division of Materials Processing Technology, Management and Computer Techniques in Materials Science, Institute of Engineering Materials and Biomaterials, Silesian University of Technology, ul. Konarskiego 18a, 44-100 Gliwice, Poland

* Corresponding author: E-mail address: miroslawa.pawlyta@polsl.pl

Received 15.02.2011; published in revised form 01.04.2011

ABSTRACT

Purpose: The aim of this study was to find out how $CeZrO_2$ and $Ni/CeZrO_2$ structures change after the steam reforming of toluene.

Design/methodology/approach: Nickel oxide supported on $CeZrO_2$ ($Ni/CeZrO_2$) with nickel loading of 10 wt. % was prepared by incipient wetness impregnation using an aqueous solution of nickel nitrate. Structure, morphology and chemical composition changes after the steam reforming of toluene were investigated by means of scanning electron microscopy (SEM), energy dispersive X-ray spectroscopy (EDS) and by X-ray diffraction (XRD) measurements. Additionally, spent $Ni/CeZrO_2$ was regenerated in O_2 while the fresh $Ni/CeZrO_2$ was subjected to two kinds of reduction: (i) in hydrogen, in order to reduce NiO to Ni and (ii) in toluene, in order to find if the reduction of NiO to Ni by C_7H_8 is followed by carbon deposition on metallic nickel.

Findings: XRD results revealed the formation of a CeO_2-ZrO_2 solid solution with a cubic symmetry. $Ni/CeZrO_2$ preparation results in the increase of crystallites in comparison to the size of the commercial $CeZrO_2$. Reduction from NiO (200) to Ni (111) in samples reduced under hydrogen and toluene was confirmed while morphology of $Ni/CeZrO_2$ remained unchanged. $Ni/CeZrO_2$ reduced under toluene include large amount of carbon, deposited by decomposition of the hydrocarbon. Steam reforming of toluene not influence on morphology of investigated materials. Energy dispersive spectroscopy indicated larger amount of carbon residuals in sample after test in comparison to fresh $Ni/CeZrO_2$. After regeneration in O_2 carbon residuals were successfully removed.

Practical implications: Nickel catalysts supported on ceria-zirconia can be efficiently applied in reforming reactions.

Originality/value: $CeZrO_2$ and $Ni/CeZrO_2$ was selected as a model compound of tar from biomass gasification.

Keywords: Nanomaterials; Catalysts; $Ni/CeZrO_2$; Steam reforming

Reference to this paper should be given in the following way:

A. Łamacz, M. Pawlyta, L.A. Dobrzański, A. Krztoń, Characterization of the structure features of $CeZrO_2$ and $Ni/CeZrO_2$ catalysts for tar gasification with steam, Archives of Materials Science and Engineering 48/2 (2011) 89-96.

MATERIALS

1. Introduction

Biomass is an important alternative energy source [1, 2]. Its main advantage over fossil fuels is neutral emission of greenhouse gases such as CO_2. Gasification (next to combustion and pyrolysis) is one of three main methods of biomass conversion [3] and it produces syngas, which can be used in the generation of electricity, production of clean fuels for transportation (e.g. methanol, dimethyl ether) and Fischer – Tropsch synthesis. Among CO and H_2, gasification products are CO_2, water, nitrogen (in the case of air application), small amounts of methane and higher hydrocarbons. The impurities present in the gas consist of ash, volatile alkali metals and tar, which can condense or polymerize to more complex structures in the pipes, filters or heat exchangers. The formation of tar is still a major problem in biomass gasificaton system because it causes process equipment problems what negatively influence on the efficiency of syngas production. Tar is a complex mixture of various hydrocarbons and its composition depends on the type of gasified material, the temperature of gasification and the equivalence ratio. According to the literature data [4-6], the main components of tar from biomass gasification are benzene, toluene, phenol, cresols and naphthalene. There are several methods of tar elimination but the reforming processes are the most promising. During catalytic steam reforming, that takes place inside the gasifier, tars are decomposed to CO and H_2, enriching gas from biomass gasification in these components.

Nickel catalysts, especially those supported on ceria or ceria-zirconia mixed oxides have been found very active and stable in reforming reactions [7-9]. However, nickel is susceptible for carbon deposition what is one of the main causes of catalyst deactivation during hydrocarbon reforming. Extensive studies on carbon deposition on nickel revealed its filamentous growth and the dependence of its morphology and chemistry on the reaction conditions and carbon source. It has been found that the growth of carbon filaments takes place by the diffusion of carbon through nickel particle, what leads to the formation of metastable carbide intermediate at the end of the filament. An alternative mechanism assumes the surface diffusion of carbon to the edges of nickel particle [10].

The aim of this study is to find out how $CeZrO_2$ and $Ni/CeZrO_2$ structures change after the steam reforming of toluene (SR), which was selected as a model compound of tar from biomass gasification [9]. Catalytic runs of SR proved high activity and stability of nickel catalyst, while the support itself has been also found active. The conversion of toluene to CO and CO_2 at 700°C reached 50 and 98% while hydrogen yield was 50 and 83% for $CeZrO_2$ and $Ni/CeZrO_2$ respectively. Additionally, spent $Ni/CeZrO_2$ was regenerated in O_2 while the fresh $Ni/CeZrO_2$ was subjected to two kinds of reduction: (i) in hydrogen, in order to reduce NiO to Ni and (ii) in toluene, in order to find if the reduction of NiO to Ni by C_7H_8 is followed by carbon deposition on metallic nickel.

2. Experimental

2.1. Catalysts preparation

The commercial ceria–zirconia mixed oxide ($CeZrO_2$) with a composition of $Ce_{0.68}Zr_{0.32}O_2$ was supplied by RHODIA Electronics & Catalysts. Nickel oxide supported on $CeZrO_2$ ($Ni/CeZrO_2$) with nickel loading of 10 wt. % was prepared by incipient wetness impregnation using an aqueous solution of nickel nitrate. After impregnation, the catalyst was dried at 110°C and calcined at 700°C in air for 2h.

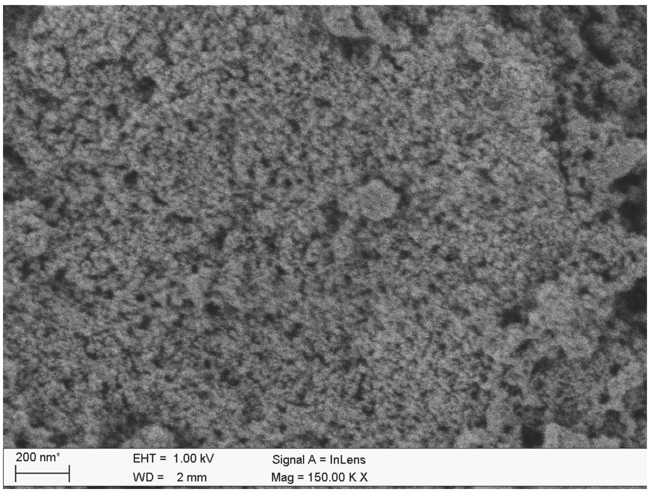

Fig. 1. SEM image of $CeZrO_2$ support

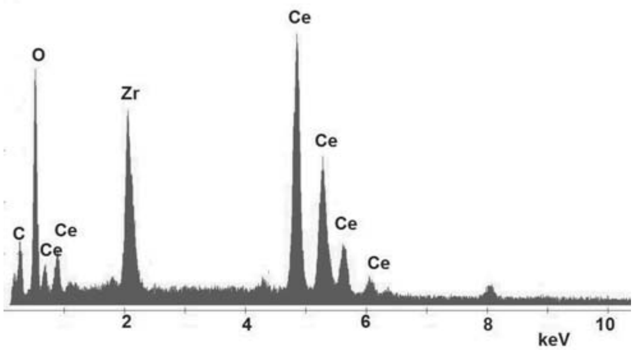

Fig. 2. EDX spectrum of $CeZrO_2$ sample imaged in Fig. 1

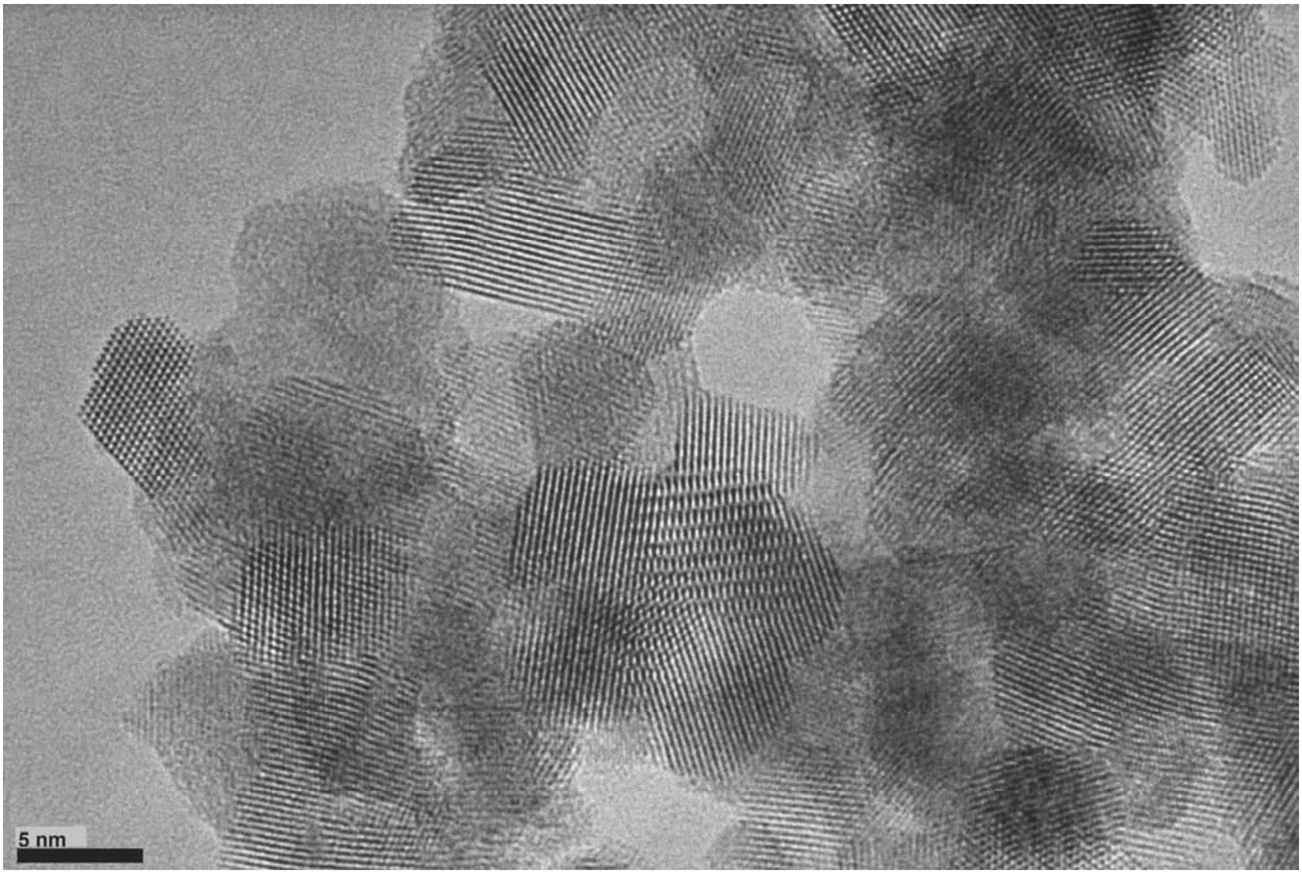

Fig. 3. HR TEM image of $CeZrO_2$ support

2.2. Catalytic tests

Catalytic runs of toluene steam reforming in steady state conditions over fresh $CeZrO_2$ and Ni/$CeZrO_2$ were carried out at 700°C for 10 h. The total flow of 250 ml/min and GHSV = 10000 h^{-1} were applied. The reaction mixture consisted of 2500 ppm of C_7H_8 and 4.2 vol. % of H_2O in argon. In order to determine the influence of toluene on Ni/$CeZrO_2$, an additional catalytic run - following described above procedure but in the absence of H_2O - was performed. Such reduction of Ni/$CeZrO_2$ in C_7H_8 lasted 3 h. The regeneration of spent (in SR) Ni/$CeZrO_2$ was carried out in 5 vol. % of O_2 in argon, at 700°C for 5 hours. The reduction of Ni/CeZrO2 was carried out in 5 vol. % of H_2 in Ar at 700 °C/ 3h.

2.3. Catalysts characterization

SEM images in SE mode were obtained using a Zeiss Supra 35 field emission SEM equipped with energy dispersive X-ray (EDX) analyzer. Ultra high resolution and precise imaging could be obtained using high efficiency In-lens SE detector working at low beam energy and at very short working distances. Samples for scanning electron microscopy were imaged without coating. TEM images were recorded using a JEOL JEM 2011 transmission electron microscope operated at 200 kV. Samples for transmission electron microscopy were prepared by dispersing powder in ethanol, placing in an ultrasonic bath, then putting droplets onto 3 mm copper grids coated with amorphous carbon film and drying in air at room temperature. The crystal structure of the catalysts were determined by powder XRD diffractometer (Panalytical X'Pert Pro, Co K_α radiation, λ = 0.1789 nm). For the determination of the position of the diffraction peaks in XRD pattern curve fitting was performed with the software program Fityk (www.unipress.waw.pl/fityk/; Levenberg–Marquardt algorithm). The goodness-of-fit was indicated by the residuals between the calculated fit curve and the observed spectrum. Determined positions of the diffraction peaks in XRD pattern were compared with JCPDS data sets to obtain crystallographic parameters.

3. Results and discussion

3.1. Catalysts

$CeZrO_2$ support is homogenous material, consisted mainly from fine particles (Fig. 1). The particles diameter can be roughly estimated to be a few dozen nanometers. The Ce, Zr and O appearance are confirmed by energy dispersive X-ray spectrometry (Fig. 2). The HRTEM image (Fig. 3) revealed that $CeZrO_2$ support consists of randomly agglomerated well crystallized sharp-edged nanoparticles of 4-10 nm size. As a thermal treatment process was applied for Ni/$CeZrO_2$ preparation it is expected that the size of crystallites should increase in comparison to the size of the commercial $CeZrO_2$. That phenomenon was confirmed by SEM observation as well as XRD measurements. Average size of the nickel oxide supported on $CeZrO_2$ particles is larger than the particles of commercial ceria–zirconia mixed oxide (Fig. 4). SEM images obtained with different magnifications disclose homogenous and porous morphology of Ni/$CeZrO_2$. Aside from Ce, Zr and O also Ni appearance is confirmed at that sample (Fig. 5). XRD patterns of $CeZrO_2$ and Ni/$CeZrO_2$ are visible in Fig. 6. The broad peaks in the XRD patterns confirm nanometric size of the crystallite in investigated materials. It is clear that crystals size in sample Ni/$CeZrO_2$ are larger than in $CeZrO_2$ sample. The average crystallite size of CeO_2 was calculated using the Debye–Scherrer formula:

$$D = \frac{K\lambda}{\beta \cos(\theta)} \tag{1}$$

in which D is the crystallite size, λ the wavelength of the X-ray radiation, K is usually taken as 0.9, 2θ is the Bragg angle of the CeO_2 (111) peak, and β is the integrated line width at half-maximum height, after subtraction of equipment broadening.

The average crystallite size of CeO_2 nanoparticles was estimated at about 6 nm for $CeZrO_2$ support and 14 nm for Ni/$CeZrO_2$. Diffraction pattern for Ni/$CeZrO_2$ sample is sufficiently distinct and for that sample crystallographic parameters could be precisely determined. Visible bands are neither characteristic of cubic ceria nor of tetragonal zirconia (Tab. 1). Determined positions of the diffraction peaks in XRD pattern with the software program Fityk (Tab. 2) were compared with JCPDS data sets to obtain crystallographic parameters. The XRD pattern of Ni/$CeZrO_2$ (Fig. 7) exhibited the lines corresponding to ceria with cubic phase shifted (for example) from 2θ = 33.3° to 2θ = 34.1°; from 2θ = 55.7° to 2θ = 57.2°; and from 2θ = 66.5° to 2θ = 68.2°. A separate zirconia phase was not detected. These results revealed the formation of a CeO_2–ZrO_2 solid solution with a cubic symmetry [11]. The lines corresponding to nickel oxide (200) was marked.

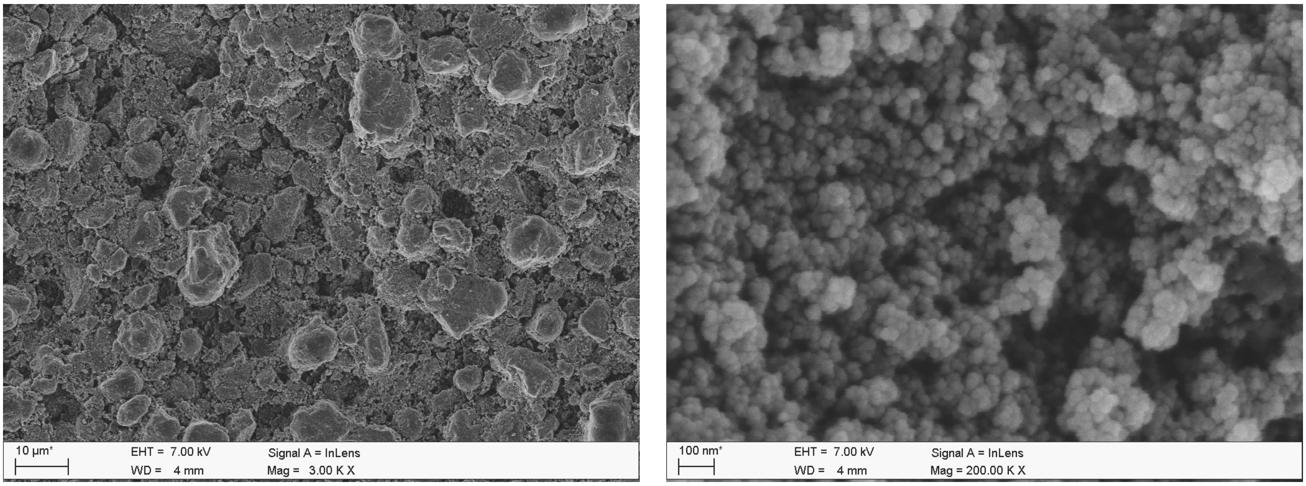

Fig. 4. SEM images of Ni/$CeZrO_2$

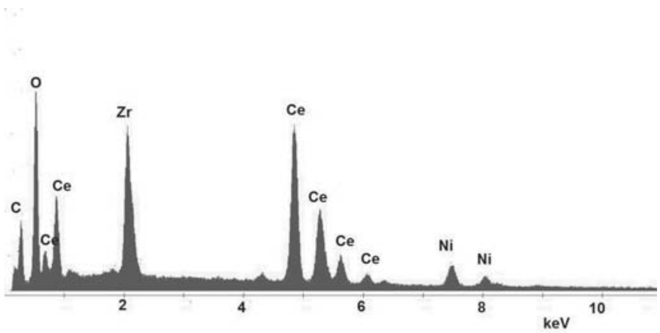

Fig. 5. EDX spectrum of Ni/$CeZrO_2$ sample imaged in Fig. 4

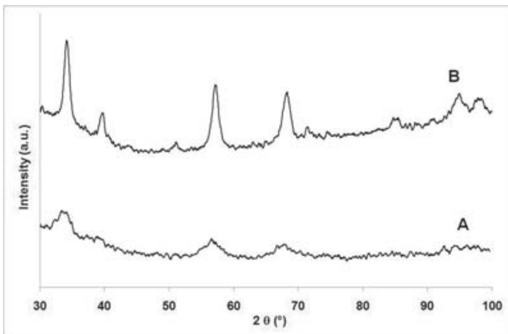

Fig. 6. XRD patterns of $CeZrO_2$ (A) and Ni/$CeZrO_2$ (B)

Table 1.
The crystallographic parameters of potential chemical components of $Ni/CeZrO_2$ sample (the Bragg angle 2θ for Co K_α radiation)

Chemical name	2θ, °	d_{hkl}, Å	hkl
Cerium Oxide CeO_2 JCPDS 81-0792	33.3	3.1	(111)
	38.6	2.7	(200)
	55.7	1.9	(220)
	66.5	1.6	(222)
	69.9	1.6	(400)
	82.8	1.4	(331)
	92.2	1.2	(420)
	95.3	1.2	(422)
Cerium Oxide Ce_2O_3 JCPDS 78-0484	30.8	3.4	(100)
	34.3	3.0	(002
	35.4	2.9	(011)
	46.8	2.3	(012)
	54.7	1.9	(110)
	62.2	1.7	(103)
	66.2	1.6	(112)
	66.9	1.6	(201)
Zirconium Oxide ZrO_2 JCPDS 88-10007	35.3	3.0	(101)
	40.6	2.6	(002)
	41.2	2.5	(110)
	59.6	1.8	(200)
	70.5	1.6	(211)
	74.7	1.5	(211)
	99.9	1.2	(301)
Nickel Oxide NiO JCPDS 78-0643	43.6	2.4	(111)
	50.7	2.1	(200)
	74.6	1.5	(220)
	90.5	1.3	(331)
	95.8	1.2	(222)
Nickel Ni JCPDS 87-0712	52.2	2.0	(111)
	61.0	1.8	(200)
	91.8	1.2	(220)

Table 2.
Calculated parameters of Lorentzian and Gaussian functions used for modeling XRD patterns of nickel oxide supported on $CeZrO_2$ ($Ni/CeZrO_2$)

Function type	Center (°)	Area (%)	Int. width (°)
Lorentzian	34.2	100	1.94
Lorentzian	39.6	29	1.77
Gaussian	51.0	5	1.15
Lorentzian	57.2	69	1.78
Lorentzian	68.2	63	2.09
Gaussian	71.7	8	1.70
Gaussian	85.0	8	1.30
Gaussian	94.8	36	2.71
Gaussian	98.2	31	2.59

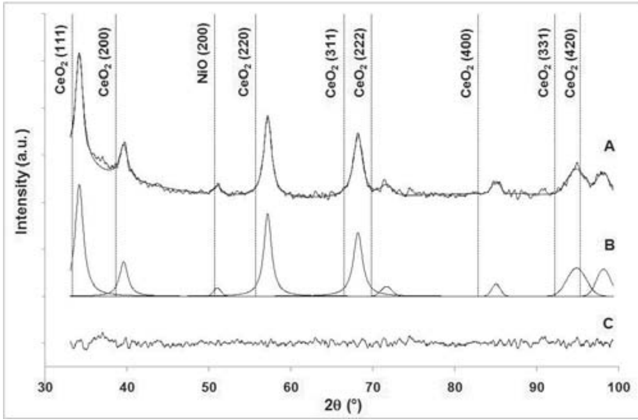

Fig. 7. XRD patterns of nickel oxide supported on $CeZrO_2$ ($Ni/CeZrO_2$) (A). Vertical lines indicate exact positions of cubic ceria and the strongest line of NiO; Lorentzian and Gaussian functions used for modeling XRD patterns by Levenberg-Marquardt algorithm (B); residuals between the calculated fit curve and the observed spectrum (C)

3.2. Reduction in hydrogen and in toluene

Fresh $Ni/CeZrO_2$ was reduced under hydrogen and toluene. Morphology of $Ni/CeZrO_2$ reduced under H_2 remained porous and homogenous (Fig. 8). Material consist of spherical particles, which are closely connected, but empty spaces with different sizes are visible. Comparison of XRD patterns of fresh $Ni/CeZrO_2$ and $Ni/CeZrO_2$ reduced under H_2 confirmed reduction of NiO to Ni (Fig. 12). Morphology of $Ni/CeZrO_2$ reduced under toluene is also porous, but more heterogenous (Fig. 9). EDX spectrum of $Ni/CeZrO_2$ reduced under toluene imaged indicate significantly larger amount of carbon at that sample (Fig. 11), in comparison to the smaller amount of carbon in $Ni/CeZrO_2$ reduced under H_2 (Fig. 10). Reduction from NiO (200) to Ni (111) is clearly present XRD patterns (Fig. 12).

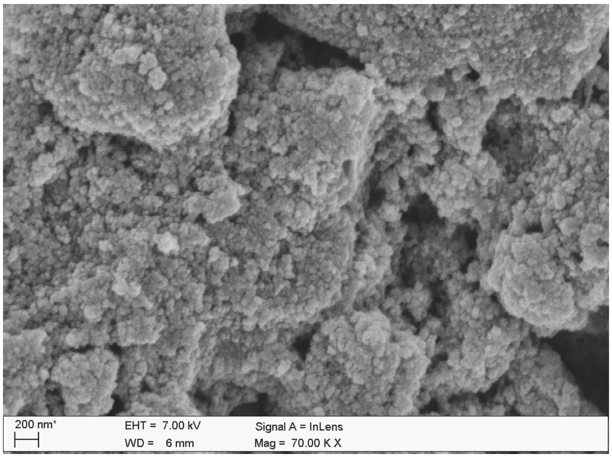

Fig. 8. SEM images of Ni/CeZrO_2 reduced under H_2

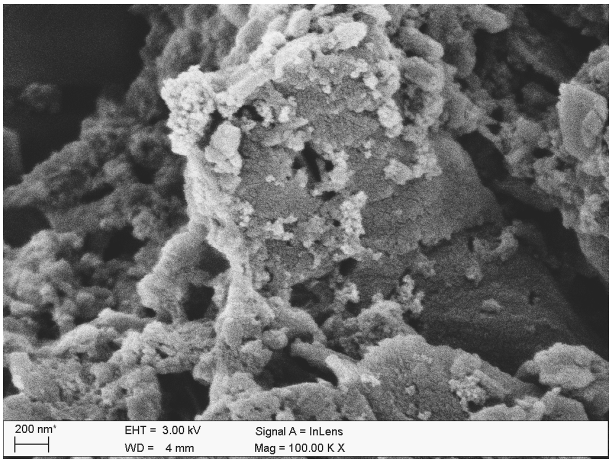

Fig. 9. SEM images of Ni/CeZrO_2 reduced under toluene

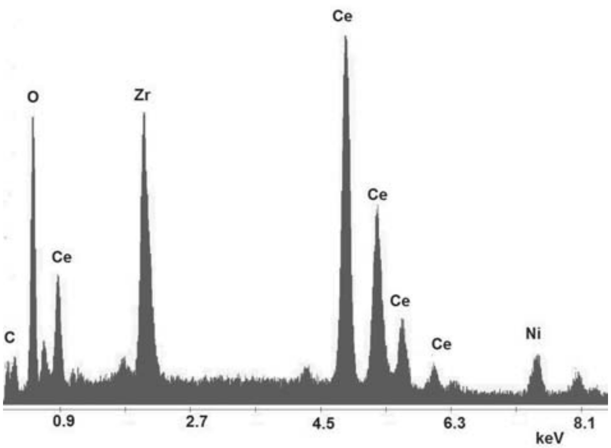

Fig. 10. EDX spectrum of Ni/CeZrO_2 reduced under H_2

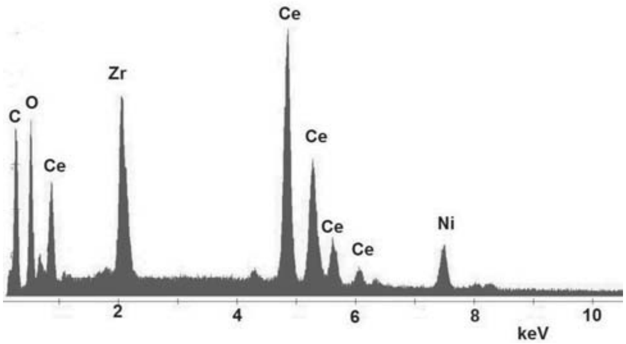

Fig. 11. EDX spectrum of Ni/CeZrO_2 reduced under toluene

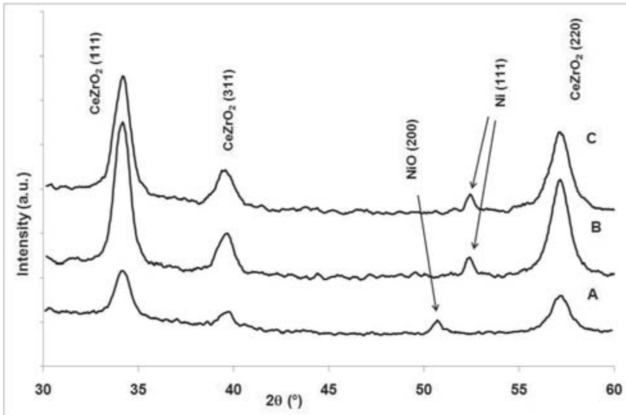

Fig. 12. XRD patterns of fresh Ni/CeZrO_2 (A), Ni/CeZrO_2 reduced under H_2 (B) and Ni/CeZrO_2 reduced under toluene (C)

3.3. Steam reforming of toluene

Morphology of catalyst didn't changed significantly after the steam reforming of toluene (Fig. 13). Sample retained initial morphology. The basic components are spherical particles closely connected with large amount of empty spaces between them. Diameter of spherical particles can be estimated to about 10-20 nm. Taking into account that the support itself has been also found active, the same experiment (the steam reforming of toluene) was performed for fresh CeZrO_2. As was expected the size of crystallites remained smaller (Fig. 14). The average crystallite size of CeO_2 nanoparticles after the steam reforming of toluene was estimated at about 13 nm for CeZrO_2 support and 15 nm for Ni/CeZrO_2. Energy dispersive spectroscopy indicated larger amount of carbon residuals in sample after test (Fig. 15) in comparison to fresh Ni/CeZrO_2 (Fig. 5).

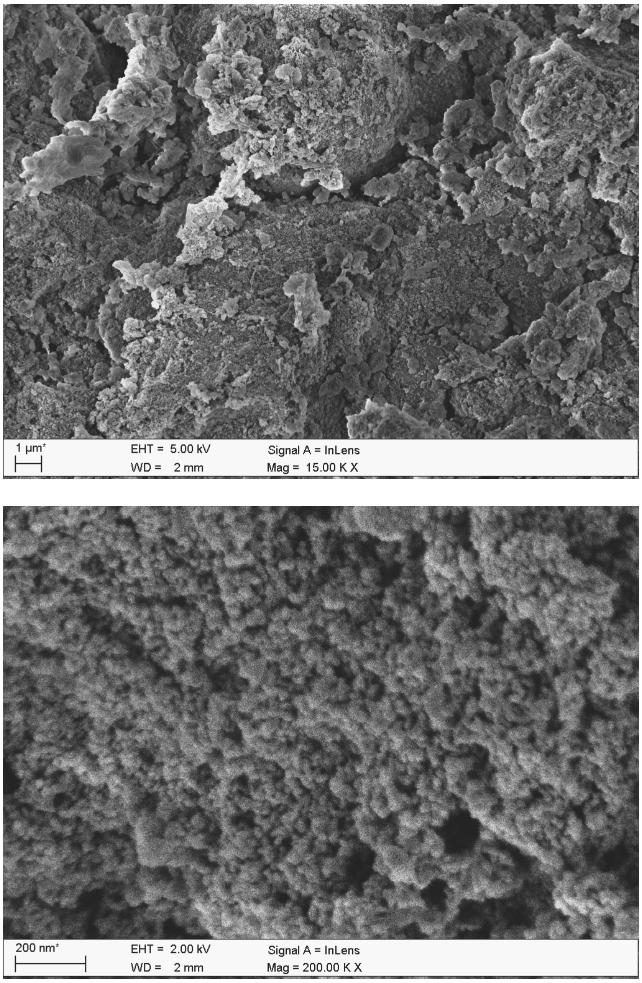

Fig. 13. SEM images of Ni/$CeZrO_2$ after the steam reforming of toluene

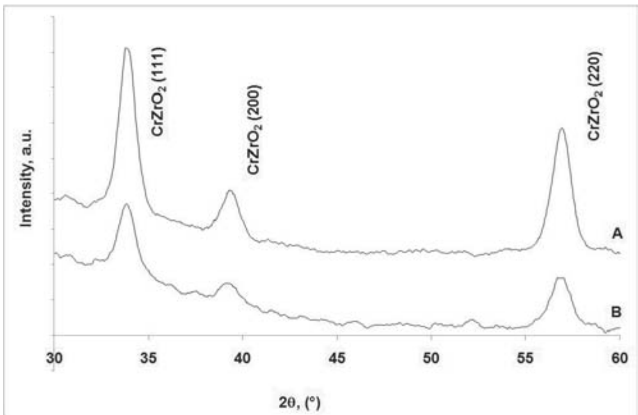

Fig. 14. XRD patterns of $CeZrO_2$ after the steam reforming of toluene (A) and Ni/$CeZrO_2$ after the steam reforming of toluene (B)

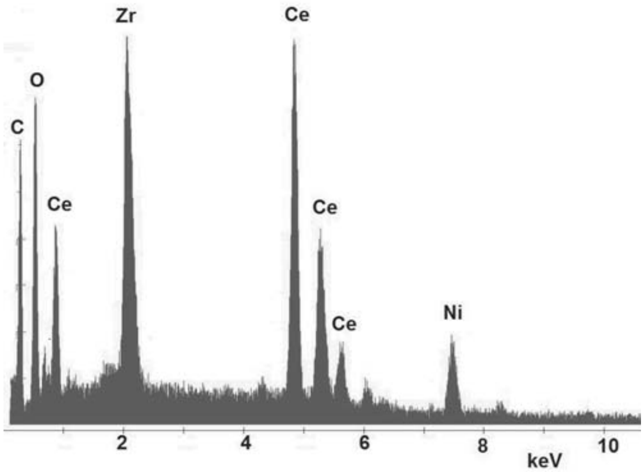

Fig. 15. EDX spectrum of Ni/$CeZrO_2$ after the steam reforming of toluene

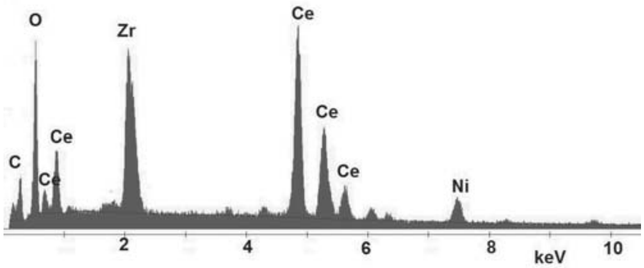

Fig. 16. EDX spectrum of spent Ni/$CeZrO_2$ regenerated in O_2

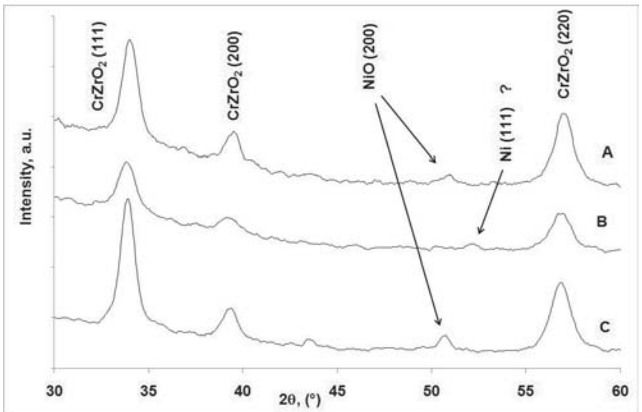

Fig. 17. XRD patterns of $CeZrO_2$ (A); Ni/$CeZrO_2$ after the steam reforming of toluene (B) and spent Ni/$CeZrO_2$ regenerated in O_2

3.4. Regeneration in O_2

Spent Ni/$CeZrO_2$ was regenerated in O_2 in order to remove carbon residuals and to oxidize metallic Ni to NiO. Carbon residuals were remove and amount of carbon in sample after regeneration is smaller (Fig. 16) then after the steam reforming of toluene (Fig. 15). Comparison of XRD patterns of $CeZrO_2$, $Ni/CeZrO_2$ after the steam reforming of toluene and spent $Ni/CeZrO_2$ regenerated in O_2 confirmed reduction of NiO to Ni and next oxidation metallic Ni to NiO (Fig. 17).

4. Conclusions and perspectives

XRD results revealed the formation of a CeO_2–ZrO_2 solid solution with a cubic symmetry. $Ni/CeZrO_2$ preparation results in increasing of crystallites in comparison to the size of the commercial $CeZrO_2$. Reduction from NiO (200) to Ni (111) in samples reduced under hydrogen and toluene was confirmed while morphology of $Ni/CeZrO_2$ remained unchanged. $Ni/CeZrO_2$ reduced under toluene include significantly larger amount of carbon than samples reduced under hydrogen. Steam reforming of toluene not influence on morphology of investigated materials. Energy dispersive spectroscopy indicated larger amount of carbon residuals in sample after test in comparison to fresh $Ni/CeZrO_2$. After regeneration in O_2 carbon residuals were sucesfully removed what proved that nickel catalysts supported on ceria-zirconia oxides can be applied in reforming reactions.

References

[1] P. Vindis, B. Mursec, C. Rozman, M. Janzekovic, F. Cus, Mini digester and biogas production from plant biomass, Journal of Achievements in Materials and Manufacturing Engineering 35/2 (2009) 191-196.

[2] L.A. Dobrzański, A. Drygała, A. Januszka, Formation of photovoltaic modules based on polycrystalline solar cells, Journal of Achievements in Materials and Manufacturing Engineering 37/2 (2009) 607-616.

[3] M. Spilka, A. Kania, R. Nowosielski, Integrated recycling technology, Journal of Achievements in Materials and Manufacturing Engineering 31/1 (2008) 97-102.

[4] J. Han, H. Kim, The reduction and control technology of tar during biomass gasification/pyrolysis: An overview, Renewable and Sustainable Energy Reviews 12 (2008) 397-416.

[5] T. Phuphuakrat, N. Nipattummakul, T. Namioka, S. Kerdsuwan, K. Yoshikawa, Characterization of tar content in the syngas produced in a downdraft type fixed bed gasification system from dried sewage sludge, Fuel 89 (2010) 2278-2284.

[6] R. Coll, J. Salvado, X. Farrioli, D. Montane, Steam reforming model compounds of biomass gasification tars: conversion at different operating conditions and tendency towards coke formation, Fuel Processing Technology 74 (2001) 19-31.

[7] B.I.N. Buffoni, F. Pompeo, G.F. Santori, N.N. Nichio, Nickel catalysts applied in steam reforming of glycerol for hydrogen production, Catalysis Communications 10 (2009) 1656-1660.

[8] A. Bampenrat, V. Meeyoo, B. Kitiyanan, P. Rangsunvigit, T. Rirksomboon, Naphthalene steam reforming over Mn-doped CeO_2–ZrO_2 supported nickel catalysts, Applied Catalysis A: General 373 (2010) 154-159.

[9] A. Łamacz, A. Krztoń, G. Djéga-Mariadassou, Steam reforming of model gasification tar compounds on nickel based ceria-zirconia catalysts, Catalysis Today (2011) doi:10.1016/j.cattod.2010.11.067 (in press).

[10] X. Chen, A.R. Tadd, J.W. Schwank, Carbon deposited on Ni/Cesingle bondZrsingle bondO isooctane autothermal reforming catalysts, Journal of Catalysis 251 (2007) 374-387.

[11] F.B. Passos, E.R. de Oliveira, L.V. Mattos, F.B. Noronha, Partial oxidation of methane to synthesis gas on Pt/CexZr1−xO_2 catalysts: the effect of the support reducibility and of the metal dispersion on the stability of the catalysts, Catalysis Today 101 (2005) 23-30.